Full 3D thermal-hydraulic and electric modelling of quench propagation in HTS conductors

Full 3D thermal-hydraulic and electric modelling of quench propagation in HTS conductors

OPEN ACCESS
IOP Publishing
Superconductor Science and Technology
Supercond. Sci. Technol. **37** (2024) 125012 (11pp)
https://doi.org/10.1088/1361-6668/ad8e8a

Full 3D thermal-hydraulic and electric modelling of quench propagation in HTS conductors

A Zappatore

NEMO Group, Dipartimento Energia, Politecnico di Torino, Torino, Italy

E-mail: andrea.zappatore@polito.it

Received 13 September 2024, revised 23 October 2024
Accepted for publication 3 November 2024
Published 13 November 2024

Abstract

A fully three-dimensional multi-physics model to simulate quench propagation in high temperature superconducting (HTS) conductors for fusion applications is presented. It accounts for thermal, electric and fluid dynamics throughout the entire transient. The need for high-fidelity models for quench simulations comes from the bulky layouts of many HTS conductors that are being proposed. The model is then validated against experimental data, showing a good agreement on all the relevant quantities (local voltages and temperatures). It is shown that the detailed model improves the quality of the agreement with the measured data with respect to more simplified models. It also allows an insight on the temperature distributions in the conductor cross-section, which can be relevant for the interpretation of experimental data as well as to support the design of quench detection strategies which rely on local temperature variations.

Keywords: quench, model, 3D, validation

1. Introduction

Quench propagation in high current conductors based on high temperature superconducting (HTS) material is an open issue due to the small normal zone propagation velocity. This makes the quench much more challenging to be detected than for conductors made of low temperature superconducting (LTS) materials. For this reason, an extensive test campaign is ongoing within the EUROfusion Consortium in order to characterize experimentally different conductors design from the quench point of view. Also, this experimental campaign aims at building a database to calibrate and validate numerical models which can then be more reliably used for the simulation of quench in full conductors and/or on different designs. Several conductors designed and manufactured by the Swiss Plasma Center (SPC) [1] and by ENEA have already been tested and others will be tested in forthcoming experiments. A calibration and validation exercise has been satisfactorily accomplished [2] modelling the quench propagation with a 1D code [3]. This modelling approach is based on lumping the cross-section of the solids and of the fluids in each axial node. This implies assigning a single value of temperature for the solids, a single value of speed, pressure and temperature for the fluids and a single value of current for the current-carrying elements.

However, this approach has some limitations, i.e. a limited capability in discretizing the cross-section of the conductor. This becomes important in the case of bulky solid structure as those foreseen in different designs of HTS cable-in-conduit conductors (CICCs) such as the 60 kA HTS conductor proposed by SPC [4], the ENEA slotted-core

conductor [5], the CroCo conductor designed by the Karlsruhe Institute of Technology (KIT) [6], VIPER conductor designed and manufactured by MIT-CFS [7] and the CORC-based conductor for fusion applications [8], to cite just some of them. All those conductors have in common a much bulkier solid structure compared to the porous structure of the ITER-like conductors [9]. This implies having much less efficient homogenization of the temperature on the cross-section during fast events like quench, see the assessment done in [10].

Few approaches have been proposed to address this difference with respect to LTS conductors. For the latter, well-established 1D codes, based on having a good homogenization of the temperature, thus of the current, in the cross-section, were developed and validated, such as 4C [11] and THEA [12]. To model HTS conductors, 1D multi-regions approaches have been developed, such as [13], for which single conductor sub-components are discretized each in multiple sub-domains in the cross-section. This was done, for example, in the case of the ENEA slotted-core quench simulations [13], where the aluminum core of the conductor was discretized in multiple sub-domains in the cross-section to account for thermal gradients arising during the quench propagation. The limitation of this approach is that is not efficient from the computational point of view and from the pre-processing point of view: the discretization of the cross-section in many sub-domains may become cumbersome (because each sub-domain needs to be 'connected' to the surrounding ones and it is difficult to automatize this process) and the burden can increase because dedicated preliminary analysis, as also done in [14], could be needed in order to assess the correct number of sub-domains needed for each conductor sub-component. Additionally, to ensure that the discretization is sufficient, the user should create different models with a growing number of sub-domains. Being these codes developed in-house, i.e. for internal use and without the availability of Graphics User Interfaces and/or optimized ways to build the input other than writing text input files, this process may be lengthy and error-prone. Furthermore, the experiments analyzed and simulated in [2] showed that the 1D approach is not able to catch the temperature of bulky structure, such as the conduit of the conductors tested. This is due to the large characteristic time for the heat diffusion, which is mainly driven by the large thickness of the solids present in these conductors, with respect to LTS conductors. This eventually leads to non-uniform temperature distribution, which cannot be reproduced if the solid components are lumped in one or too few regions.

Other approaches were based on a 2D (axial-radial) approximation of the conductor [15], whose main limitation is the need to have axisymmetric conductors, which is not typically the case.

Hybrid modelling approaches have been proposed, such as those based on a 2D + 1D discretization of the conductor: with a given spacing, the cross-section of the conductor was discretized in 2D while the axial direction was approximated in 1D [16]. In this case, the limitation comes from the need of having several 2D cuts in the quenching region, but the closer they get, the worse the 2D + 1D approximation becomes, because the heat conduction between adjacent cuts would not be negligible anymore. Additionally, as the quench propagates, the 2D cuts should follow the quench front, i.e. changing the position of the cuts during the transient itself, which make the implementation of this strategy for quench simulations quite cumbersome.

The need for accurate modelling of quench propagation in HTS conductors for fusion is a priority for many research groups or companies because of the difficulty in detecting the quench itself. Therefore, an accurate reproduction of the quench during the real operation of the magnet could help developing or assessing new or existing detection strategies.

In this work, a fully three dimensional thermal-hydraulic and electric model is developed and validated against available experimental results. This model is then capable of accounting for any three dimensional effect which may be due to the solid bulky structures, anisotropy of the tape properties or local thermal and electric contacts among the conductor sub-elements.

The enabling technology for the development of such models is the availability nowadays of high performance computing infrastructure as well as the capability of commercial software to easily (from the user perspective) perform parallel computations, thus lowering the computational cost of each simulation.

This work is focused on the modelling of one of the conductor recently tested in SULTAN for which quench experimental data are published in [2], i.e. the non-twisted one, for the sake of simplicity as the anisotropy of the critical current density does not play a role due to the absence of twisting. Nevertheless, the model being developed is fully 3D, thus it can easily account for a 3D distribution of the critical current density.

The conductor under analysis features three HTS stacks of tapes. Each stack is enclosed in a copper profile, constituting a triplet of HTS 'strand'. The triplet is then enclosed in a thick steel conduit (or jacket) which provides mechanical support and containment for the He forced flow. In fact, the coolant can flow in the interstitials among the strands and the conduit, see figure 1. The conductor was equipped with voltage taps on the external surface of the jacket as well as with temperature sensors. Also, temperature sensors were placed in the He stream in the same location of the jacket temperature sensors, see again figure 1. More details on other layouts can be found in [1].

The quench was induced by warming up the He at the inlet with a dedicated electric heater on the feeding pipe. The quench then is initiated in the so-called High Field Zone (HFZ), i.e. where the SULTAN background magnetic field reaches its peak, which is uniform for about 40 cm, see figure 1.

The aim of this work is to (1) develop a fully 3D transient and multi-physics model which is able to simulate the quench propagation in HTS conductors relevant for fusion applications and (2) validate it against experimental data. In section 2, the 3D model is described, focusing on the electric, fluid and thermal physics, then in section 3 the comparison

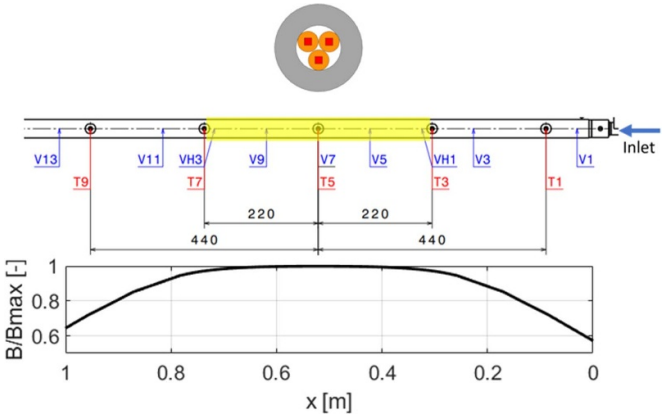

Figure 1. On top, section view of the non-twisted conductor tested in the quench experiment in SULTAN. The dark orange squares are the stacks of REBCO tapes, the light orange round regions are the copper profiles in which the stacks are enclosed, the white regions are the voids where helium flows and the grey conduit is the jacket. In the center, zoom of the diagnostics in the first meter of the conductor, showing the voltage taps (V) in blue and the temperature sensors (T) in red. The High Field Zone (HFZ) is highlighted in yellow. The helium inlet in indicated on the right. In the bottom, the normalized profiled of the background magnetic field is shown.

with the experimental data and the discussion of model results is presented.

2. 3D model

The 3D model couples the electric, fluid and thermal physics, which are the three aspects which come into play during the initiation and propagation of quench in forced-flow (HTS) CICCs. The model has been implemented in the commercial software Siemens STAR-CCM+ [17] and all the models are solved using finite volume approximation. The user-defined functions and solver settings are discussed and highlighted this section. This software was chosen mostly because it handles well the solution of the fluid flow, which is critical in this kind of conductors and challenging from the numerical point of view due to the strong variations of the helium properties during the quench propagation.

2.1. Electric model

The electric potential distribution in each cell of the domain is computed from (1)

$$\int_A \sigma \nabla \phi \, \mathrm{d}A = 0 \tag{1}$$

where ϕ is the (scalar) electric potential, σ is the electric conductivity and A is the cell face of a generic cell of the discretized domain. The electric resistivity of the copper as a function of the temperature, magnetic field and RRR and of the stainless steel as function of the temperature are taken from [18].

The electric resistivity in the HTS stack is computed as an equivalent resistivity ρ_{eq} from the parallel of the copper stabilizer of the tapes in the stack and the superconductor according to (2)

$$\rho_{\mathrm{eq}} = \frac{\rho^{\mathrm{om}}_{\mathrm{Cu,tapes}} \rho_{\mathrm{SC}}}{\rho^{\mathrm{om}}_{\mathrm{Cu,tapes}} + \rho_{\mathrm{SC}}} \tag{2}$$

where $\rho^{\mathrm{om}}_{\mathrm{Cu}}$ is the homogenized copper resistivity and ρ_{SC} is the superconductor resistivity. This is done in order to account for the presence of the copper layers in the tapes of the stack. Neglecting the presence of this copper would lead to an overestimation of the resistivity, hence of the resistance, of the HTS stack once the superconductor quenches. The copper resistivity is weighted over the ratio between the stack (A_{stack}) and stabilizer ($A_{\mathrm{stabilizer}}$) contained in the tapes of the stack cross-sectional areas according to (3)

$$\rho^{\mathrm{om}}_{\mathrm{Cu}} = \rho_{\mathrm{Cu}}(B,T,RRR) \cdot \frac{A_{\mathrm{stack}}}{A_{\mathrm{stabilizer}}} \tag{3}$$

where B is the magnetic field intensity, T is the temperature and RRR is the residual resistivity ratio (here assumed equal to 100).

The weighting is adopted because the resistivity ρ_{eq} is then assigned to the entire stack volume in the model, thus in this way the value of the resistance is preserved.

The superconductor resistivity or, equivalently, its conductivity, can be defined from the power law reported in (4) according to (5) or (6), respectively,

$$E = E_{\mathrm{C}} \left(\frac{J}{J_e(B,T)} \right)^n \tag{4}$$

$$\rho_{\mathrm{SC}} = \frac{E_{\mathrm{C}}}{J_e(B,T)} \left(\frac{\|\mathbf{J}\|}{J_e(B,T)} \right)^{(n-1)} \tag{5}$$

$$\sigma_{\mathrm{SC}} = \frac{E_{\mathrm{C}}}{J_e(B,T)} \left(\frac{\|\mathbf{E}\|}{E_{\mathrm{C}}} \right)^{1-\frac{1}{n}} \tag{6}$$

where $\boldsymbol{E}$ is the electric field, E_C is the critical electric field ($= 100\,\mu\mathrm{V\,m^{-1}}$), n is the n-value ($= 14$), $J_e(B,T)$ is homogenized value of the critical current density defined according to (7), following the same rationale described for $\rho^{\mathrm{om}}_{\mathrm{Cu}}$, $\boldsymbol{J}$ is the current density. The dependence of J_e on θ, i.e. the angle between the (background) magnetic field with respect to the tape c-axis, is not reported because the stacks are not twisted and the magnetic field is perpendicular to the wide tape face throughout the conductor length,

$$J_e = J_{\mathrm{C}}(B,T) \cdot \frac{A_{\mathrm{SC}}}{A_{\mathrm{stack}}} \cdot f(x) \tag{7}$$

In (7), $J_{\mathrm{C}}(B,T)$ is the critical current density, A_{SC} is the superconductor cross-sectional area and $f(x)$ is a function that takes into account the experimental distribution of the critical

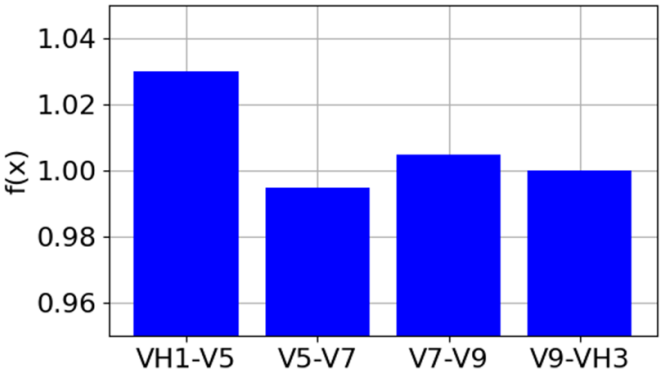

Figure 2. Distribution of the ratio between the local critical current and the average value of the critical current in the HFZ.

current in the HFZ, see figure 2. This was computed from the local voltage measurements in the HFZ (VH1-V5, V5-V7, …) from which it is possible to retrieve a local value of I_C. The resulting distribution of I_C (normalized with respect to the average I_C in the HFZ) is reported in figure 2 and it has been implemented in the model, since few percent of variation in the I_C can affect the position where the quench is initiated and how the quench propagates in the HFZ.

The choice between (5) and (6), although mathematically equivalent, is crucial from the numerical point of view: equation (6) must be preferred since it computes the (strongly non-linear) electric conductivity of the superconductor through the electric field, which is computed as $\mathbf{E} = -\nabla\phi$ from the electric potential ϕ, which is in turn the variable computed by the electric solver, see (1). On the other hand, the use of (5) requires the computation of $\mathbf{J}$ through the Ohm's law ($\mathbf{E} = \rho\mathbf{J}$), thus involving the resistivity, which for the superconductor is strongly non-linear: this adds instability to the iterations when the quench is propagating, which, from the numerical point of view, becomes a stiff problem. To cope with this instability an extremely small time-step would be needed, e.g. smaller than 1 μs. Therefore, the use of (6) is preferred as it allows to go to time-steps of the order of 1 ms without showing instabilities in the electric field computation when the quench is propagating.

The parameters of the scaling law adopted for the definition of $J_C(B,T)$ (taken from [19] and reported in (8) and (9)) are listed in table 1,

$$J_C(B,T) = \frac{A}{B} B_c(T)^{\beta} \left(\frac{B}{B_c(T)}\right)^{p} \left(1 - \frac{B}{B_c(T)}\right)^{q} \quad (8)$$

$$B_c(T) = B_{c20m}\left(1 - \frac{T}{T_{c0m}}\right)^{\alpha}. \quad (9)$$

The magnetic field is the background field of SULTAN, which has a peak value of 10.9 T in the HFZ. It is much larger than the self-field, which is therefore neglected. The temperature is computed by the thermal model. The volumetric heat source due to Joule effect is computed by the electric model according to $q = \mathbf{J}\cdot\mathbf{E}$. The HYPRE [20] solver is adopted for the solution of (1).

Table 1. Parameters for the REBCO scaling law.

Parameter	REBCO
T_{c0m} [K]	90
B_{c20m} [T]	132.5
A [A·T/m^2]	$1.464 \cdot 10^8$
p [−]	0.5875
q [−]	1.7
α [−]	1.54 121
β [−]	1.96 679

2.2. Thermal model

The thermal model solves the 3D transient heat conduction equation. This equation is coupled to the fluid temperature one (see next sub-section) as well as to the electric one, as the Joule heating becomes the heat source as soon as the current sharing between the stack and the other conductive material begins.

All the thermophysical properties are temperature dependent and, in case of copper, the thermal conductivity depends also on the magnetic field and RRR [18]. The density and specific heat capacity of the stacks of tapes are homogenized according to the mass and heat capacity, respectively, based on the composition of the layer of the tapes and of the solder among them. The anisotropy of the thermal conductivity of the stack is taken into account according to the measurement reported in [21].

2.3. Fluid model

The fluid model solves the full set of Navier–Stokes equations, computing the velocity, pressure and temperature of the helium in the voids where it flows, see figure 1. The presence of turbulence is accounted for using the k-ω SST model [22] for its closure. In order to cope with the strong non-linearities of the helium thermophysical properties, which are taken from the CoolProp database [23], accounting for the dependence on the temperature and pressure, a coupled approach has been chosen as solver of the set of equations: this algorithm solves the fluid equations all at the same time, as opposed to the so-called segregated approach, which solves one equation at a time (using the so-called inner iterations). The drawback of the coupled approach is a larger memory requirement than the segregated approach (although the memory employed by this model is not too demanding, as discussed in the appendix), but it provides more stability to the algorithm, see [24], chapters 5 and 12. Since the pressure and especially the temperature variations are very large (causing then a large variations also in the thermophysical properties) in the problem at hand, the coupled approach is preferred.

2.4. Solver coupling strategy

The schematics of the coupled physics implemented in the 3D model is shown in figure 3. The heat equation is solved computing the temperature of the solids, which is then used to compute the electric conductivity and the heat flux to the

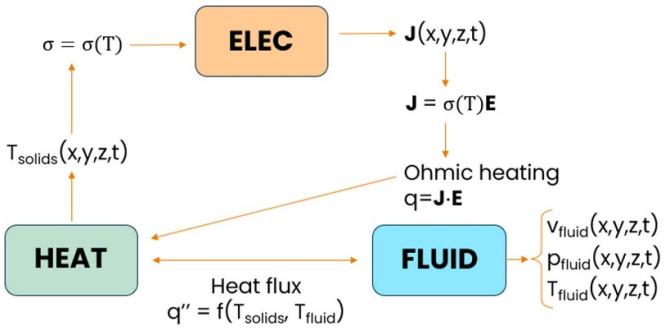

Figure 3. Schematics of the different physics (thermal or heat diffusion, electric and fluid) solved for in the model implemented. The variables computed by each physics and exchanged among those are also shown.

fluid, which in turn depends also on the fluid temperature. This is computed by the fluid model, together with the fluid velocity and pressure, accounting for the forced-flow and turbulent nature of the coolant. The electric solver, receiving the electric conductivity as function of the solid temperature as input and the electric field of the previous time-step, computes the electric potential and, through the Ohm's law, the current density. At this point the Joule heating is computed and it is passed to the heat equation as heat source and the next time step begins.

Concerning the time step, it was implemented an adaptive time stepping strategy based on the variation of the current density between two consecutive time steps. The only built-in strategies are based on the Von Neumann number (adapting the time step on the solution of the temperature in the solids) and on the Courant number (adapting the time step based on the velocity of the fluid). As the most sensitive physics during the quench initiation and propagation is the electric one, due to the strong non-linearity of the power law, a user-defined parameter f_{adapt} was defined. It is based on the variation between two consectuive time steps of the current density in the computational domain as reported in (10)

$$f_{\text{adapt}} = \sqrt{\sum_{i=1}^{N_{\text{cells}}} \left(\frac{\|\mathbf{J}\|_i^{t+\Delta t} - \|\mathbf{J}\|_i^{t}}{\|\mathbf{J}\|_i^{t}} \right)^2} \tag{10}$$

where t is the the previous time instant, Δt is the time step and i is the generic cell of the domain.

After a parametric study, two thresholds were fixed, as a compromise between accuracy and computational cost, adapting the time step as follows: in case f_{adapt} is smaller than 12, then the time step is increased by a factor 1.1; in case f_{adapt} is larger than 18, then the time step is decreased by a factor 0.8; if it falls between the two thresholds, then the time step is not varied. A minimum time step of 10 μs and a maximum one equal to 0.1 s were set. During the initial phase of the quench propagation, i.e. when a non-negligible current still flows into the superconductor, the time step varies monotonically from 0.1 s down to 0.4 ms. Then, when the current variation is less pronounced, i.e. the quench propagates more slowly and in the quenched region all the current flows into the normal conducting materials, the time step slightly increases up to 1 ms and it stays there until the simulation is terminated, i.e. when the maximum total voltage reaches the same value reached during the experiment.

2.5. Interfaces, boundary and initial conditions

The relevant interfaces of the thermal model are those between different thermal regions and the parameter of interest is the thermal contact resistance between the different regions. The thermal contact between the HTS stack and the copper profile is assumed to be perfect, i.e. with zero thermal resistance at their interface. The assumption is motivated by the fact that the stack is soldered, thus the solder should ensure a good thermal contact to the copper profile. On the other hand, the thermal contact between the copper profile and the jacket is certainly worse because it is simply a line-contact. The corresponding thermal resistance is assumed to be equal to that found calibrating the 1D model in [2], i.e. $R_{\text{th}} = 0.083\,\text{m} \cdot K/W$.

The boundary conditions set in the thermal model on the external surfaces are adiabatic or symmetry, according to the surface considered, see figure 4.

The interfaces of interest concerning the fluid model are those with the solids, especially because at the interface fluid-solid the heat transfer from/to the fluid takes place. The advantage of using an high-fidelity model is that the heat transfer coefficient is not an input taken from, e.g. semi-empirical correlations, as in the 1D models, but it is consistently computed from the solution of the Navier–Stokes equations. Nevertheless, a suitable computational grid is needed to this aim, see section 2.6.

To set the boundary conditions in the fluid model, the inlet and outlet pressures were set such that the mass flow rate in correspondence of the initial steady state equals the experimental one. The corresponding pressure drop is equal to 26 Pa, with an inlet pressure of 10.2 bar. This kind of boundary condition is an approximation since of the pressure is not constant throughout the transient. Nevertheless, it is the condition that more closely reproduce the experimental behavior of the mass flow rate when the warm helium enters the conductor. The alternative would have been to set at the inlet a mass flow rate taken from the experiment. However, during the quench, backflow takes place, which cannot be measured by the same sensor used to measure the inlet mass flow rate, thus the numerical model could not see the backflow if the measured mass flow rate is imposed. On the other hand, if the pressure is fixed at the inlet, this allows the presence of backflow in the model when the helium pressurizes in the conductor more than the inlet pressure, e.g. during quench propagation.

The electric contact resistance between the HTS stack and the surrounding copper is set constant and equal to $R_{\text{el}} = 5 \cdot 10^{-10}\ \Omega \cdot \text{m}^2$, which is the resistance times the contact area, while the contact resistance between the copper and the stainless steel of the jacket is set to $R_{\text{el}} = 4.2 \cdot 10^{-8}\ \Omega \cdot \text{m}^2$. These values were calibrated against another quench test which

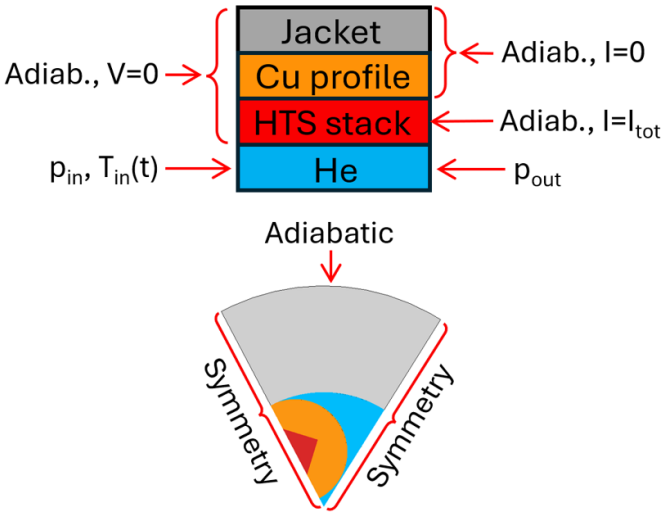

Figure 4. Schematics of the boundary conditions for the different physics on the different sub-domains. On top, the boundary conditions on the inlet and outlet sides are reported (Adiab. stands for adiabatic, V = voltage, I = current, p_{in} and T_{in} are the inlet pressure and temperature, p_{out} = outlet pressure). On the bottom, the boundary conditions on the external sides are reported.

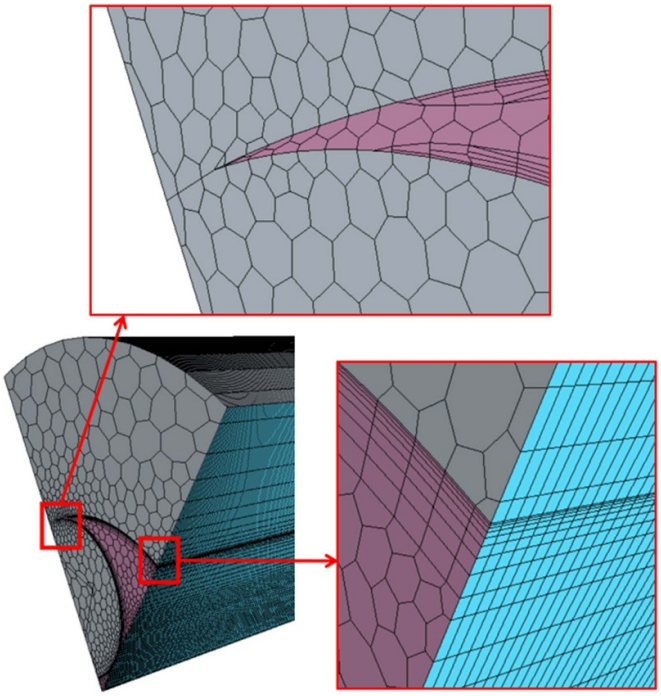

Figure 5. View of the computational grid close to one of the end of the computational domain. The inset on top shows the detail of the prismatic layer close to the geometrical singularity of the fluid domain. The inset on the right shows the beginning of the mesh in the axial direction, which is constructed extruding the polygonal mesh in several layers.

reached lower temperatures than those of the quench simulated and discussed in section 3.

The boundary conditions of the electric model consist in fixing the voltage to 0 on all the conducting materials on the HFZ side (=He inlet side) and imposing the total current on the stack surface on the He outlet side, see again figure 4. Given the symmetry considered, i.e. half of one of the three stacks, the current imposed in the model is equal to 2500 A, since no asymmetry in the current sharing among the three stacks was observed during the experiment. On the external boundaries along the conductor, a symmetry or an insulating boundary condition is imposed.

The initial conditions must be prescribed in terms of the computed variable, i.e. the electric potential, velocity, pressure and temperature of the fluid and temperature of the solids. For the electric potential, a pre-solver is adopted, before starting the actual iterations. The pre-solver iterates for a given number of iterations or until a given tolerance is reached, only solving for the electric potential. In this initialization phase, the current density in the superconductor is set as constant, in order to avoid the non-linearity given by (6). This allows computing an initial electric potential distribution coherent with the initial current distribution, avoiding numerical oscillations in the first iterations. The initial velocity of the fluid is set knowing the mass flow rate, the helium cross-section and the helium density, while the initial pressure and temperature are set to 10.2 bar and 6.7 K, respectively. The initial temperature of the solids is set to 6.7 K.

2.6. Computational grid

A further challenge to be tackled in the solution of the fluid problem is the solution of the boundary layer to correctly account for the friction with the wall and especially the heat transfer with the solids. The latter is relevant in the first phase of the quench initiation and propagation, when the heat capacity of the helium is still large, i.e. below 20–30 K. To accurately solve the boundary layer, a prismatic type of cells is used in the fluid mesh close to the solid walls, see figure 5. At the same time, to avoid too skewed cells close to the contact between the copper profile and the jacket, the prismatic cells are suppressed, in order to keep a good quality in each region of the mesh.

Both in the fluid and in the solids, the polyhedral mesh constructed on the inlet surface is extruded in several layers towards the outlet. This approach allows saving lot of cells with respect to meshing the entire geometry with polyhedral cells.

To optimize further the number of cells, the number of layers in the axial direction is finer in the HFZ (with a thickness of the layers in the rage 3–6 mm), while they are gradually expanded towards the outlet, where the magnetic field drops, thus where it is not expected to have quench.

In order to find the best compromise between accuracy and computational cost, a grid independence study was performed varying the number of cells in the domain either varying the polygonal cells in the inlet surface or varying the number of prism layer to resolve the boundary layer. Due to the computational burden of such study, a simplified case was simulated only on the fluid region imposing a localized steady state

Table 2. Grid independence study in the fluid region. Reported values of mass flow rate and maximum temperature are at steady state.

Total cells	Prism layers	dm/dt [g/s]	$T_{\max}$ [K]
245 400	4	1.566	57.55
375 000	8	1.386	55.31
891 410	16	1.340	55.99
4548 688	8	1.407	54.35
8173 332	8	1.402	54.76

heat flux on the boundary corresponding to the interface with the copper profile in the full model, approximating the heat deposited at a given instant during the quench as seen by the fluid. The key parameters, i.e. mass flow rate and peak temperature in the fluid are reported in table 2. The minimum number of prism layers to accurately compute the mass flow rate was estimated to be 8 and a corresponding total number of cells equal to 375 000 is considered to give the best compromise between accuracy in the computation of key results and speed of the computation (directly driven by the number of cells).

3. Results

In this section, the model validation against experimental data is reported. After that, the main outcomes of the model are discussed.

3.1. Validation against experimental data

The accuracy of the proposed model is checked against the available experimental data reported in [2]. The available measurements are the voltage and the helium and jacket temperatures. Also, the copper temperature between two voltage taps can be estimated from the measured voltage, assuming that all the current is transported by the copper itself. Knowing the dependence of the copper resistivity on the temperature, the latter can be computed analytically by solving the implicit equation $\Delta V = \rho(T)\, L/A_{\mathrm{Cu}} \cdot I_{\mathrm{tot}}$ for the temperature. Being an indirect measurement, this is commonly called 'virtual thermometry'.

3.1.1. Voltage and maximum temperature evolution. The measured and computed voltage are compared in figure 6: the agreement is good, especially where the largest voltage is reached, i.e. V7–V9 and V9–VH3. The first couple of taps in the HFZ (VH1–V5) shows a larger measured voltage while the last one (V9–VH3) is slightly overestimated by the computed solution; this implies that the computed normal zone is slightly shifted towards the outlet.

Nevertheless, as a direct consequence of the good match between the measured and computed voltages in the HFZ, also the comparison between the computed and measured maximum temperatures is very satisfactory, see figure 7. The experimental 'virtual temperature' starts only at 100 K,

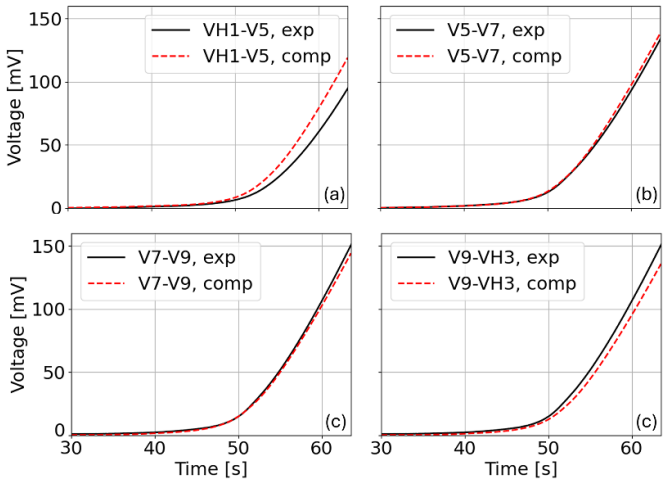

Figure 6. Evolution of the experimental and computed voltage between voltage taps (a) VH1–V5, (b) V5–V7, (c) V7–V9 and (d) V9–VH3.

i.e. when the voltage is sufficiently high so that the assumption that all the current is flowing in the copper in the quenched region is reasonable. The computed maximum temperature is taken as the volume average of the copper temperature over the same length covered by the voltage taps considered (V5–V7 and V7–V9).

3.1.2. Jacket temperature evolution. The comparison between the measured and computed jacket temperature in different locations is reported in figure 8. As computed values, the maximum and minimum temperature on the external surface of the jacket are reported. In all the locations shown, the values computed by the 3D model bracket the experimental value, throughout the transient. Here is where the 3D nature of the temperature distribution is clear, thus the 1D approximation fails: the evolution of the jacket temperature computed by the 1D model (adopted in [2]) systematically overestimates the measured value, up to 20 K when the measured value is 40 K, thus leading to a remarkable error. To correctly catch the jacket temperature evolution, a much more detailed model is needed, such as that presented here.

3.2. Temperature distributions

The 3D model allows investigating the local 3D distribution of the temperature in the jacket and in the helium. The temperature in the superconductor as well as in the copper is mostly uniform due to their large thermal conductivity and good thermal contact, thus its distribution is less interesting than those in the jacket and in the helium. Indeed, the temperature difference in the stack and in the copper is 4 K when the hotspot is reached.

3.2.1. Jacket temperature. The temperature in the cross-section at $x = 0.5$ m (center of the HFZ) of the jacket at $t = 63$ s (when the maximum temperatures are reached), is shown in figure 9. It is clearly shown the non-uniformity of

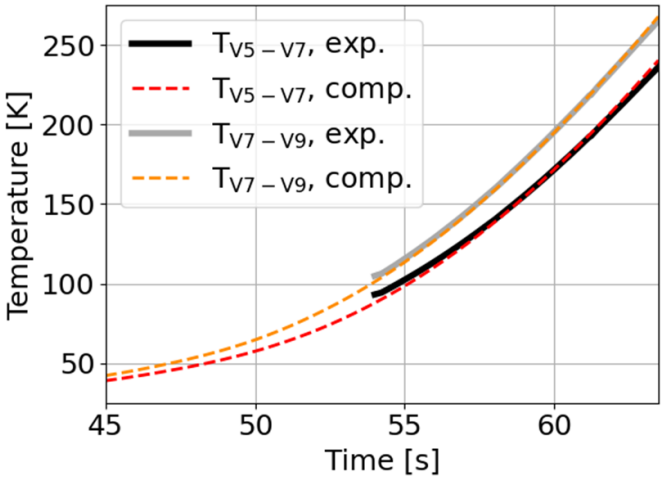

Figure 7. Comparison between the virtual temperature reconstructed from the voltage measured by taps V5–V7 and V7–V9 and the computed volume-averaged temperature in the strand.

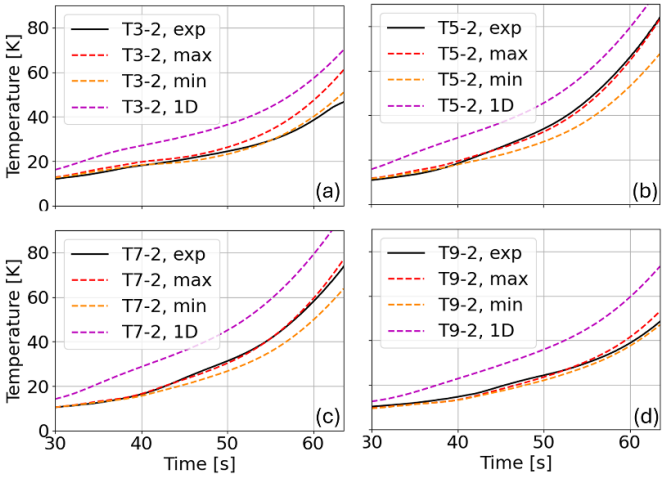

Figure 8. Evolution of the experimental jacket temperature, of the maximum and minimum temperature on the external surface of the jacket computed by the 3D model and that computed with the 1D model in correspondence of (a) T3–2, (b) T5–2, (c) T7–2 and (d) T9–2.

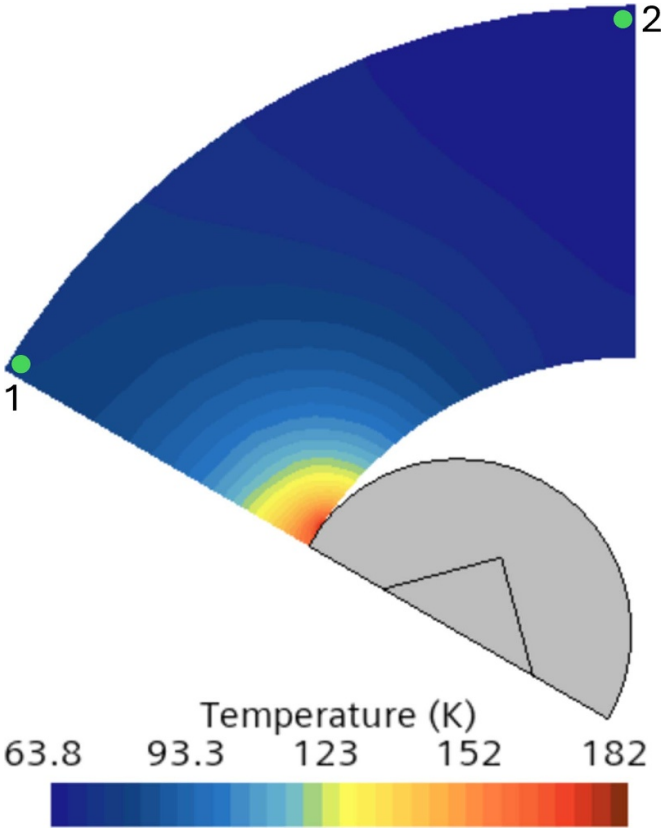

Figure 9. Computed temperature distribution in the jacket at $x = 0.5$ m, $t = 63$ s. The strand is reported in grey for reference. The two points where the temperature on the external surface of the jacket is monitored and discussed in the text are highlighted in green.

the temperature in the jacket: it is strongly peaked where it is in contact with the strand (which reaches $T = 253$ K), while the minimum is reached on the external surface with a temperature difference of more than 115 K. This is a direct consequence of the low thermal diffusivity of the stainless steel. It is clear that a unique value of the temperature as assumed by the 1D model (in the cross-section), in this case is a bad assumption. To capture this distribution with a 1D model, the cross-section should be discretized in several 'shells' in the radial direction as well as in several 'chunks' in the azimuthal direction, making the model very difficult to handle and build.

This result shows the relevance of a 3D thermal-hydraulic and electric model to simulate fast transients in bulky HTS conductors: based on these results, one could reliably evaluate the effectiveness on different positions of alternative quench detection strategies, e.g. fiber optics [25] and superconducting wires [26]. Also, the 3D temperature distribution could become the input for thermo-mechanical models to analyze the possible impact of the secondary stresses due to the peaked temperature distribution on the superconductor performance and its possible degradation (as it was observed after these quench experiments).

The comparison of the measured temperature on the external surface of the jacket with the computed one, shown in figure 8 as function of time, is shown also as function of the axial coordinate in figure 10. The temperature computed on the two green points shown in figure 9 brackets the measured one quite well, see figure 10. For reference and comparison, also the virtual temperatures (reconstructed from the experiment and computed) are reported, showing that the the computed temperature in the strands agrees very well not only with that between V5–V7 and V7–V9 as shown in figure 7 but throughout the HFZ and beyond.

3.2.2. Helium temperature. The temperature in the helium flow at $x = 0.5$ m and $t = 63$ s is reported in figure 11. The 3D model of the coolant flow allows discussing the actual temperature distribution in the helium with no approximation as in, e.g. a 1D model, and with a good level of accuracy, given the validation against experimental results discussed in section 3.1.

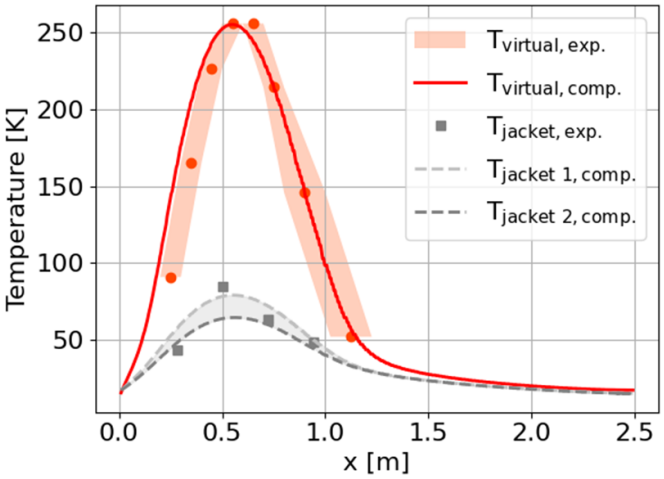

Figure 10. Jacket and superconductor temperature profiles at $t =$ 63 s. The two jacket temperatures reported refer to the two green points shown in figure 9. The superconductor temperature is taken in the center of the stack. The virtual experimental temperature refers to the temperature reconstructed from the voltage measurements. Being an average temperature between the voltage taps, it is represented as an area rather than as a line.

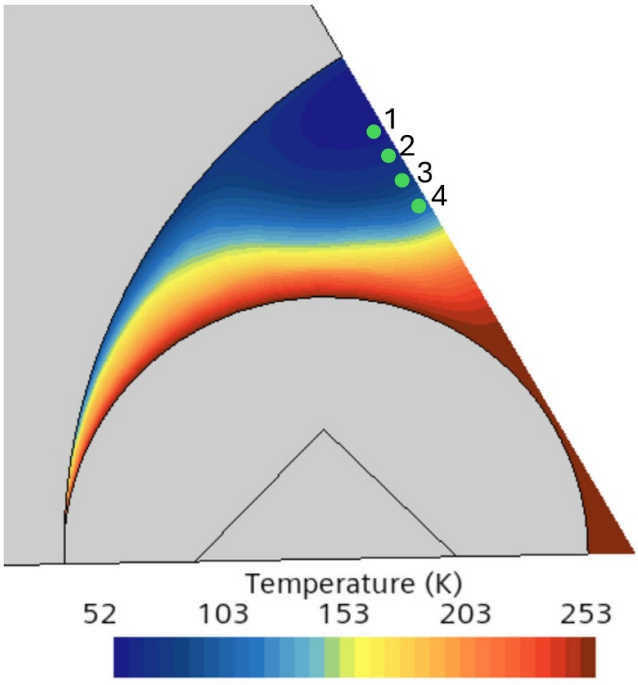

Figure 11. Computed temperature distribution in the helium at $x =$ 0.5 m, $t = 63$ s. The strand and the jacket are reported in grey for reference. The four points where the temperature is monitored and discussed in the text are highlighted in green.

The temperature in the helium cross-section is clearly non-uniform as it is in contact with the strands and the jacket, which are at very different temperatures. Note that the large temperature difference is not limited only to the close vicinity to the strands, but it involves the entire cross-section. In addition, the 3D model allows taking into account the different topology of the helium channels present in this conductor. In particular,

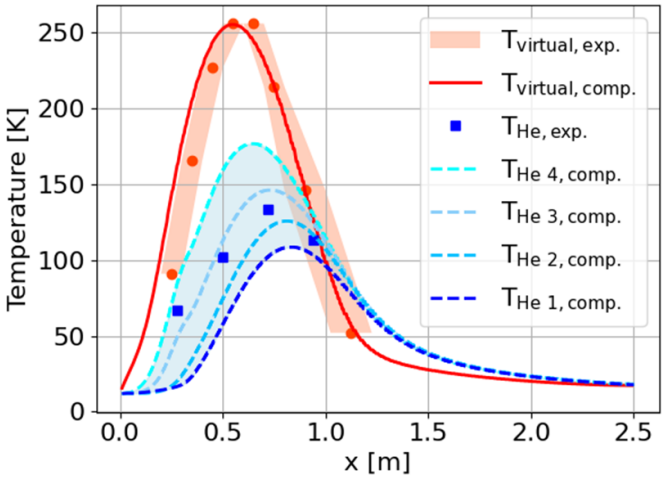

Figure 12. Helium and superconductor temperature profiles at $t =$ 63 s. The four computed helium temperatures reported refer to the four green points shown in figure 11. The superconductor temperature is taken in the center of the stack. The virtual experimental temperature refers to the temperature reconstructed from the voltage measurements. Being an average temperature between the voltage taps, it is represented as an area rather than as a line.

the small gap in the center between the three strands (bottom right in figure 11) is at a much higher temperature than the larger gap between the two strands and the jacket. To account for this effect, one should model at least two different fluid regions in the 1D model, which, especially in case they are in hydraulic contact, may lead to numerical issues due to the mass exchange.

The measured helium temperature data are compared to the computed ones in figure 12. It is shown that, taking the temperature at four different locations (reported in figure 11) which are each only 0.5 mm apart, the temperature profile changes remarkably. This helps interpreting the measured data, as the computed profile that matches better the measured one is that positioned 2.5 mm from the jacket. Nevertheless, even a difference of 0.5 mm would have changed the measured temperature by several tens of K. In this respect, together with the temperature reconstructed from the voltage measurements, the 3D model can help in retrieving the actual hotspot temperature reached in the superconductor, as that measured in the helium is closer to that with respect to the jacket temperature, but it is still $\sim$100 K lower.

4. Conclusions and perspective

A new fully 3D transient multi-physics (thermal-hydraulic and electric) model for the simulation of quench propagation in HTS conductors for fusion applications has been presented. The developed model has been validated against the quench experiment performed in SULTAN on a high current and high field HTS conductor, showing a good agreement between the computed and measured voltage and temperatures. The added value of the 3D model with respect to more simplified models is shown in particular on the comparison with

the measured jacket temperature, which is bracketed by the 3D model results, while it was systematically overestimated by the simplified models. Also, it supported the interpretation of experimental data, e.g. the helium temperature, showing that a difference of a fraction of mm in the position of the temperature sensor would have led to very different results.

The 3D model can help giving feedbacks to the design of alternative quench detection which are sensible to local temperature differences, such as fiber optics or superconducting wire quench detection, and to thermo-mechanical analysis, which, receiving as input the 3D temperature map during the quench, could computed the strain map, trying to understand the degradation mechanisms due to quench, which was experimentally observed in several conductors. Furthermore, this model can be extended to the magnet scale in order to simulate the quench propagation where 3D effects are relevant, such as in non-insulated magnets.

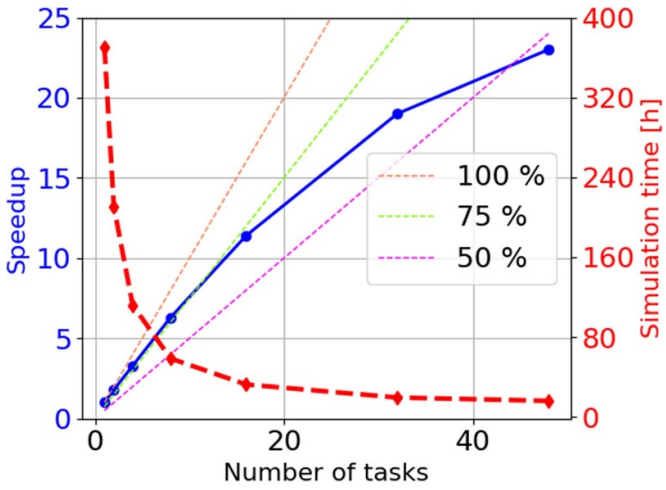

Figure 13. Computational performance of the proposed model in terms of speedup and total simulation time. The dashed lines are the reference for different level of speedup scaling efficiency.

Data availability statement

The data cannot be made publicly available upon publication because they are owned by a third party and the terms of use prevent public distribution. The data that support the findings of this study are available upon reasonable request from the authors.

Acknowledgments

The author wish to thank Nikolay Bykovskiy for useful discussions. Computational resources provided by hpc@polito (www.hpc.polito.it) and by the CINECA Marconi-Fusion cluster.

Appendix

The computational performance of the model presented in this work are discussed in this appendix, as they are relevant also to extrapolate the computing needs to different and more complex geometries.

To assess the scalability of this model on an high performance computing infrastructure (equipped with Intel(R) Xeon(R) Platinum 8160 CPU @ 2.10 GHz chips), the simulation was run for a fixed number of 'pre-iterations' (being a transient model, these are to be intended as time-steps) and then for a given number of 'sample iterations'. The former are not sampled in order to avoid perturbations in the actual computation time given by the loading of the model and of its packages or to the domain split to the different cores. The time taken by the simulation to perform the prescribed 'sample iterations' (in this case, 10 time-steps during the quench propagation) with the given number of cores allocated is stored before increasing the number of cores.

The performance of this model are quantified first in terms of speedup, defined as the ratio between the time needed to perform the sample iterations on one core and the time needed for the same task on N cores. The ideal speedup scaling would follow the 100% line plotted in figure 13. As shown, the model follows the 75% line with a low number of cores and then it tends toward the 50% line. This is a good performance, considering that the model involves different physics. In addition, the optimal number of cells per core mentioned by the software manual is around 1 million cells. Considering that this model contains in total less than 2 million cells, it means that the larger the number of cores, the less optimal the cell count per core. Therefore, larger models should scale better than this one when a larger number of cores is employed.

Another evaluator of the computational performance of a numerical model is the simulation time, i.e. an absolute measure of the time taken by the simulation to perform a run, rather than a relative comparison as that given by the speedup. This quantity was extrapolated from the time taken to perform 10 time-steps with the tested number of cores and multiplied by the total number of steps taken to complete an entire simulation. This should give an idea of the time needed to complete the entire simulation using different number of cores. It is shown in figure 13 that the time drops from few hundred hours to just 15 h in case 48 cores were used. This means that the model could still run on a workstation, as with 16 cores it takes roughly 30 h to complete a run. However, larger models would require more cores, thus requiring the use of clusters to perform the simulations in a reasonable time.

Larger models may be needed for example to account for the twisting, as that would make the geometry not symmetric. However, increasing the cell-count by a factor 6, would make its speedup better at large number of cores, partially compensating for the increased number of cells.

Concerning the RAM requirements, this is not an issue, even considering that a coupled approach for the solution of the linear system was used: the model took roughly 3 Gbytes of RAM when run with only one core up to 18 GBytes when run with 48 cores.

ORCID iD

A Zappatore https://orcid.org/0000-0001-7308-0273

References

[1] Dicuonzo O, Kang R, Sedlak K, Stepanov B, Uglietti D, Wesche R and Bruzzone P 2021 Upgrade and commissioning of the SULTAN facility to host quench experiments on HTS high current conductors *IEEE Trans. Appl. Supercond.* **31** 1–5

[2] Zappatore A, Bonifetto R, Bruzzone P, Corato V, Dicuonzo O, Kumar M, Sedlak K and Stepanov B 2023 Quench experiments on sub-size HTS cable-in-conduit conductors for fusion applications: data analysis and model validation *Cryogenics* **132** 103695

[3] Zappatore A, Heller R, Savoldi L, Wolf M J and Zanino R 2020 A new model for the analysis of quench in HTS cable-in-conduit conductors based on the twisted-stacked-tape cable concept for fusion applications *Supercond. Sci. Technol.* **33** 065004

[4] Uglietti D, Wesche R and Bruzzone P 2014 Design and strand tests of a fusion cable composed of coated conductor tapes *IEEE Trans. Appl. Supercond.* **24** 1–4

[5] Celentano G, De Marzi G, Fabbri F, Muzzi L, Tomassetti G, Anemona A, Chiarelli S, Seri M, Bragagni A and Della C A 2014 Design of an industrially feasible twisted-stack HTS cable-in-conduit conductor for fusion application *IEEE Trans. Appl. Supercond.* **24** 1–5

[6] Wolf M J, Ebner C, Fietz W H, Heller R, Nickel D and Weiss K P 2021 High temperature superconductors for fusion applications and new developments for the HTS CroCo conductor design *Fusion Eng. Des.* **172** 112739

[7] Hartwig Z S *et al* 2020 VIPER: an industrially scalable high-current high-temperature superconductor cable *Supercond. Sci. Technol.* **33** 11LT01

[8] Weiss J, van der Laan D, Radcliff K, Bagrets N, Lange C, Allen S, Holt J, Alsworth I, Daniels P and Dieudonne Y 2023 Performance of low-loss demountable joints between CORC® cable-in-conduit-conductors at magnetic fields up to 8 T developed for fusion magnets *Supercond. Sci. Technol.* **36** 085002

[9] Mitchell N *et al* 2021 Superconductors for fusion: a roadmap *Supercond. Sci. Technol.* **34** 103001

[10] Zappatore A, Fietz W H, Heller R, Savoldi L, Wolf M J and Zanino R 2019 A critical assessment of thermal–hydraulic modeling of HTS twisted-stacked-tape cable conductors for fusion applications *Supercond. Sci. Technol.* **32** 084004

[11] Savoldi R L, Casella F, Fiori B and Zanino R 2010 The 4C code for the cryogenic circuit conductor and coil modeling in ITER *Cryogenics* **50** 167–76

[12] Bottura L, Rosso C and Breschi M 2000 A general model for thermal, hydraulic and electric analysis of superconducting cables *Cryogenics* **40** 617–26

[13] Zappatore A, Augieri A, Bonifetto R, Celentano G, Marchetti M, Vannozzi A and Zanino R 2021 Development of the H4C model of quench propagation in the ENEA HTS cable-in-conduit conductor *IEEE Trans. Appl. Supercond.* **31** 1–5

[14] Sedlak K and Bruzzone P 2015 Results and analysis of the hot-spot temperature experiment for a cable-in-conduit conductor with thick conduit *Cryogenics* **72** 9–13

[15] Casali M, Breschi M and Ribani P L 2015 Two-dimensional anisotropic model of YBCO coated conductors *IEEE Trans. Appl. Supercond.* **25** 1–12

[16] Savoldi L *et al* 2016 Thermal–hydraulic modeling of a novel HTS CICC for nuclear fusion applications *IEEE Trans. Appl. Supercond.* **26** 1–7

[17] Siemens Digital Industries Software 2021 Simcenter STAR-CCM+, version 2021.1

[18] Drexler E S, Reed R P and Simon N J 1992 Properties of copper and copper alloys at cryogenic temperatures (Washington DC: NIST Monograph 177, U.S. Government Printing Office)

[19] Heller R, Gade P V, Fietz W H, Vogel T and Weiss K P 2016 Conceptual design improvement of a toroidal field coil for EU DEMO using high-temperature superconductors *IEEE Trans. Appl. Supercond.* **26** 1–5

[20] hypre: high performance preconditioners (available at: https://github.com/hypre-space/hypre)

[21] Bagrets N, Goldacker W, Jung A and Weiss K P 2013 Thermal properties of rebco copper stabilized superconducting tapes *IEEE Trans. Appl. Supercond.* **23** 6600303

[22] Menter F R 1994 Two-equation eddy-viscosity turbulence models for engineering applications *AIAA J.* **32** 1598–605

[23] Bell I H, Wronski J, Quoilin S and Lemort V 2014 Pure and pseudo-pure fluid thermophysical property evaluation and the open-source thermophysical property library coolprop *Ind. Eng. Chem. Res.* **53** 2498–508

[24] Ferziger J H, Perić M and Street R L 2020 *Computational Methods for Fluid Dynamics* (Springer)

[25] Salazar E E *et al* 2021 Fiber optic quench detection for large-scale HTS magnets demonstrated on VIPER cable during high-fidelity testing at the SULTAN facility *Supercond. Sci. Technol.* **34** 035027

[26] Bykovskiy N, Bajas H, Dicuonzo O, Bruzzone P and Sedlak K 2023 Experimental study of stability, quench propagation and detection methods on 15 kA sub-scale HTS fusion conductors in SULTAN *Supercond. Sci. Technol.* **36** 034002